

ORIGINAL ARTICLE

Open Access



Influence of Charging Oil Condition on Torque Converter Cavitation Characteristics

Cheng Liu^{1,2*} , Meng Guo¹, Qingdong Yan^{1,3} and Wei Wei^{1,2}

Abstract

Cavitation inside a torque converter induces noise, vibration and even failure, and these effects have been disregarded in previous torque converter design processes. However, modern torque converter applications require attention to this issue because of its high-speed and high-capacity requirements. Therefore, this study investigated the cavitation effect on a torque converter using both numerical and experimental methods with an emphasis on the influence of the charging oil feed location and charge pressure. Computational fluid dynamics (CFD) models were established to simulate the transient cavitation behaviour in the torque converter using different charging oil pressures and inlet arrangements and testing against a base case to validate the results. The CFD results suggested that cavitating bubbles mainly takes place in the stator of the torque converter. The transient cavitation CFD model yielded good agreement with the experimental data, with an error of 7.6% in the capacity constant and 7.4% in the torque ratio. Both the experimental and numerical studies showed that cavitation induced severe capacity degradation, and that the charge pressure and charging oil configuration significantly affects both the overall hydrodynamic performance and the fluid behaviour inside the torque converter because of cavitation. Increasing the charge pressure and charging the oil from the turbine-stator clearance were found to suppress cavitation development and reduce performance degradation, especially in terms of the capacity constant. This study revealed the fluid field mechanism behind the influence of charging oil conditions on torque converter cavitation behaviour, providing practical guidelines for suppressing cavitation in torque converter.

Keywords: Torque converter, Cavitation, CFD, Transient flow

1 Introduction

A torque converter transfers rotating power through the interaction of the fluid and the cascades. Torque converters can provide continuous speed and torque ratios, moreover, it can produce effective damping to protect the transmission system from torsional vibration, thus it is extensively used in automatic transmissions and other hydraulic transmission systems [1]. A typical automotive torque converter includes three wheels: the pump, which is driven by the engine and energises the fluid; the turbine, which discharges the fluid and drives the

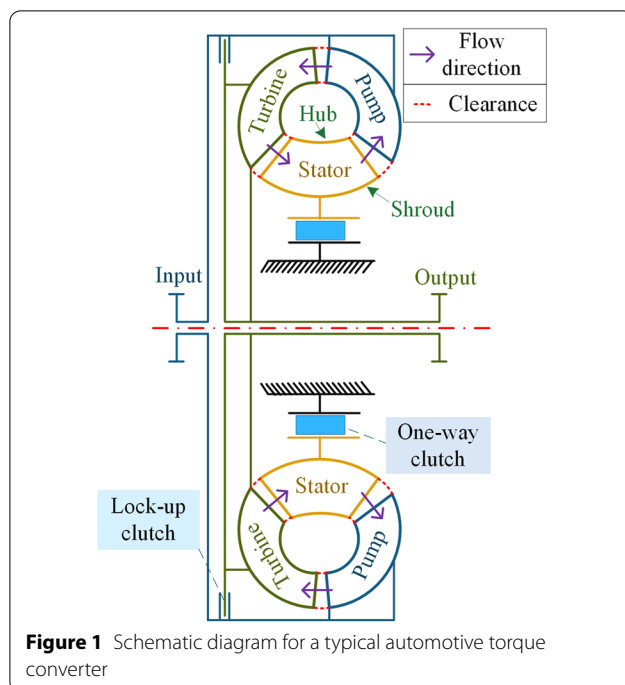
transmission; and the stator, which is fixed to a one-way clutch (Figure 1). These three components operate in close proximity to one another and form a circuit, with the working media cycling through the pump, turbine, and stator. The one-way clutch allows the stator to rotate freely to improve efficiency, and the lock-up clutch further increases the efficiency to nearly one by locking the pump and the turbine [2].

Automatic transmissions have recently been trending towards increased power density to reduce fuel consumption, leading to greater demand for smaller torque converters with a higher capacity [2, 3]. These trends require higher flow velocity in the torque converter, which leads to lower local pressures and thus greater cavitation risk [4, 5]. Cavitation has plagued fluid machinery for centuries [6, 7], degrading performance

*Correspondence: liucheng@bit.edu.cn

¹ School of Mechanical Engineering, Beijing Institute of Technology, Beijing 100081, China

Full list of author information is available at the end of the article



and introducing noise, vibration, and even failure depending on the cavitation degree [8]. Considerable research effort has been devoted to the understanding of cavitation mechanism and suppression of cavitation effects [9–11]. Cavitation in torque converters has been reported decades ago [12, 13], and continuous efforts have been put into the investigation and control of cavitation in torque converters [14].

One team conducted extensive experimental studies on torque converter cavitation. The microwave telemetry technique [15] and the nearfield acoustic test approach [16] were proposed to investigate cavitation phenomena in a series of torque converters. In another approach, Robinette et al. tested a matrix of torque converters and developed a dimensionless model for predicting cavitation [17]. Reynolds measured the sound power level in torque converters over various speed ratios and developed a response surface model to estimate the sound power of a working torque converter [18]. Watanabe et al. used transparent elements to visualize the generation and collapsing of cavitating bubbles in a torque converter at the stall and captured cavitation phenomena inside the stator over various pump speeds, concluding that cavitation may be responsible for high-frequency torque vibrations [19]. Yan et al. [20] and Rivera [21] measured the pressure in the rotor and stator of the torque converter by wireless and wired methods, and put forward the relationship between pressure fluctuation frequency and the rotating speed with different numbers of blades.

Because cavitation is inherently transient and small in scale, significant computing power is required for the precise prediction of cavitation in torque converters. Although computational fluid dynamics (CFD) models have been extensively and effectively used in real-world cases, only recently has numerical research been reported on torque converter cavitation. Ju et al. investigated the cavitation phenomena in an automotive torque converter over various speed ratios using a periodic steady-state CFD model. It was reported that cavitation mainly took place in the stator and severely degraded torque capacity [22]. Tsutsumi et al. also established a periodic steady-state CFD model to study the influence of cavitation on torque converter hydrodynamic performance [23] and concluded that the stator was prone to cavitation at lower speed ratios, whereas the flow in the pump would cavitate at higher speed ratios when ambient pressure was further reduced. Usui et al. [24] introduced a gaseous cavitation model into a commercial flow analysis software, and reproduces the position of blade erosion under conditions. Liu et al. revealed the influence of the blade profile on torque converter cavitation behaviour using a fixed turbine-stator steady-state CFD model, and then improved performance by redesigning the turbine blade to reduce cavitation [25]. The team then studied the effect of the stator blade geometry on the cavitation characteristics with a periodic steady-state CFD model. It was found that the stator blade count, leaning angle, and blade nose shape significantly affected the torque capacity loss, cavitation range, and cavitation degree [26]. The team also proposed a cavitation suppression technique by cutting a slot on the stator blades. A full three-dimensional cavitation model was built to evaluate the transient cavitation behaviour over different slot configurations, and the results showed that the addition of a slot on the stator blade can suppress the cavitation degree [27].

Most of the previous research on this topic focused either on cavitation-induced issues such as performance degradation, noise, and vibration, or on empirical design models for cavitation control. However, little is known about the influence of charging oil conditions on cavitation characteristics. In general, the effects of cavitation have been disregarded in past torque converter design processes, and modern torque converter applications require greater attention to this issue because of its high-speed and high-capacity requirements. Therefore, the study presented here used CFD modelling to investigate the influence of charging oil pressure and inlet configuration on transient cavitation characteristics. The full flow passage geometry was extracted from a base torque converter model and a refined mesh was adopted to capture transient cavitating flows. Different CFD models were developed in ANSYS CFXTM to predict the torque

converter fluid behaviour based on Reynolds-averaged Navier-Stokes equations. The Rayleigh-Plesset model was implemented to capture the formation and collapse of cavity bubbles inside the torque converter. Because the cavitating flows varied greatly in scale with different charging conditions, and because the working medium flowed in a closed-loop, the CFD calculation was slow to converge. Non-cavitation, cavitation, steady-state and transient models were performed in sequence using previous results as initial conditions to improve convergence. CFD simulations with different charging oil pressures and inlet arrangements were carried out to study the influence of charging oil conditions on the cavitation characteristics. The base model torque converter was tested under different charging conditions to validate the numerical results. Thus, this study revealed the influence of charging conditions on the transient cavitating flows inside a torque converter and provides practical guidelines to suppressing cavitation in a torque converter by controlling the charge pressure and optimizing the charging oil inlet configuration.

2 Methodology

2.1 Geometry Model

The base model was a die cast converter with a high power density, as is used in off-road vehicles. The model's torus diameter was 400 mm; the blade cascades are depicted in Figure 2.

In this model, the pump blade is highly twisted and the stator blade is relatively short, leading to a high mass flow rate and high power capacity. The three components are very close to each other, with a minimum clearance of 3

mm, and the heat produced inside the torque converter can be removed by supplying oil through the clearances between adjacent components, referred to as the pump-turbine clearance (P-T clearance), the turbine-stator clearance (T-S clearance), and the stator-pump clearance (S-P clearance). In real applications, this torque converter supplies oil through the S-P clearance and the charge pressure was 0.6 MPa.

2.2 CFD Models

Previous research reported that cavitating bubbles mainly occurred in the stator and that the stall operating condition was the worst-case scenario [28]. Thus, this study focused on the transient cavitation behaviour at stall, when both the stator and the turbine are stationary. Therefore, a turbine-stator fixed model was employed to simplify the CFD calculation. The leakage between different components and compressibility of the working medium were ignored, and the fluid was considered isothermal.

The three components were distributed into two domains: the rotating pump domain and the stationary turbine-stator domain. This simplification eliminated the interface between the stator and the turbine, reducing the demand for computer resources and improving convergence. The clearance between adjacent domains on the shroud was extracted as illustrated in Figure 3. An opening boundary was applied on the selected clearance to simulate different charging oil conditions.

The pump rotated at 2000 r/min, and the turbine-stator domain was fixed to stationary, in accordance with the test condition. A non-cavitation steady-state calculation was run first, followed by a cavitation steady-state CFD simulation based on the non-cavitation results. Lastly, a transient CFD calculation with cavitation was fulfilled using the steady-state cavitation outcome as the initial condition.

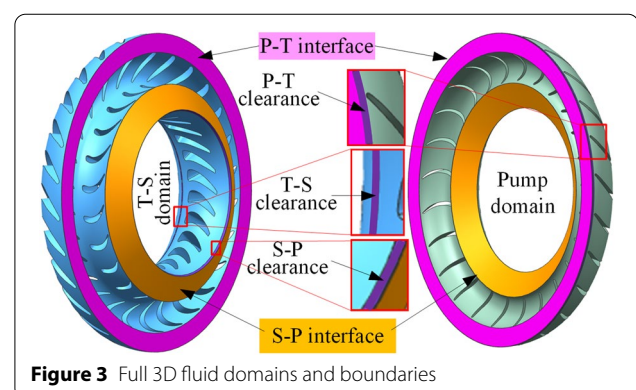
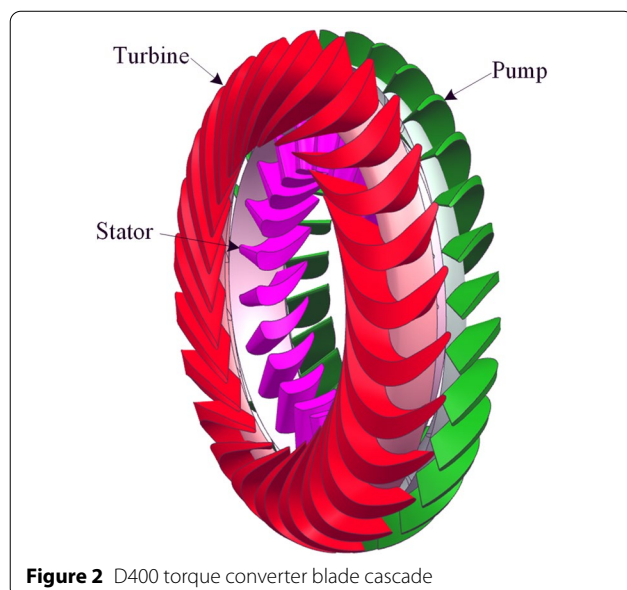


Table 1 Non-cavitation CFD settings

Analysis type	Steady-state
Fluid properties	$\rho_l = 830 \text{ kg}\cdot\text{m}^{-3}$, $\mu_l = 9\text{e}-3 \text{ Pa}\cdot\text{s}$
Turbulence model	Shear stress transport (SST)
Advection scheme	High resolution
Convergence target	RMS $1\text{e}-6$
Interface model	Frozen rotor
Boundary details	No-slip and smooth wall

2.2.1 Non-Cavitation CFD Model

The inherently unsteady flows and, the closed-loop configuration both deteriorate the convergence of the cavitation calculation; therefore, the non-cavitation CFD simulation was performed to provide a reasonable initial condition for the cavitation calculation. The detailed non-cavitation CFD settings are listed in Table 1.

Due to the existence of highly turbulent flow and strong reverse pressure gradient, a sophisticated turbulence model is needed to accurately simulate the turbulent flow behaviour. The shear stress transport (SST) model is a robust two-equation eddy-viscosity turbulence model that can simulate the flow turbulence by a combination of $k-\omega$ model and $k-\varepsilon$ model. Therefore, the SST model was employed to accurately capture the wall bounded turbulent flow. The frozen rotor interface model was applied to transfer the fluid properties between different components, and no-slip smooth walls were applied on all other boundaries except the opening.

2.2.2 Cavitation CFD Model

A steady-state model considering cavitation was established to provide appropriate initial results, and then a transient cavitation CFD simulation was carried out to capture the dynamic cavitation behaviour. A vapour was added to the CFD model, and the Rayleigh-Plesset equation was implemented to govern the mass transfer between the non-condensable liquid phase and the gas phase:

$$\frac{\partial}{\partial t}(f_l \rho_l) + \frac{\partial}{\partial x_j}(f_l \rho_l v_j) = \dot{m}, \quad (1)$$

where f_l represents liquid volume fraction, ρ_l is the fluid density, v_j is velocity, and \dot{m} represents interphase mass transfer per unit.

By ignoring the interphase slip and heat transfer, the growth of a spherical vapour bubble can be modelled by the simplified Rayleigh-Plesset equation [29]

$$\frac{dR_B}{dt} = \sqrt{\frac{2}{3} \frac{p_v - p}{\rho_l}}, \quad (2)$$

where R_B is bubble radius, p_v represents vapour pressure, and p is local pressure.

The mass transfer rate during vapourization can then be written as

$$\dot{m} = \frac{3f_v \rho_v}{R_B} \sqrt{\frac{2}{3} \frac{p_v - p}{\rho_l}}, \quad (3)$$

where f_v represents vapour volume fraction, and ρ_v is vapour density.

Given that the vapourization process is much faster than the condensation process, different equations are used to govern the two processes:

$$\begin{cases} \dot{m}^- = -F_{\text{vap}} \frac{3f_{\text{nuc}}(1-f_v)\rho_v}{R_B} \sqrt{\frac{2}{3} \frac{p_v - p}{\rho_l}}, \\ \dot{m}^+ = F_{\text{cond}} \frac{3f_v \rho_v}{R_B} \sqrt{\frac{2}{3} \frac{p - p_v}{\rho_l}}, \end{cases} \quad (4)$$

where f_{nuc} is the volume fraction of the nucleation site, F_{vap} is the vapourization constant, and F_{cond} represents the condensation constant.

The detailed model settings and the empirical coefficients for the vapourization (\dot{m}^-) and condensation (\dot{m}^+) are reported in Table 2.

Because the computing cost of capturing the inter-phase boundaries would be prohibitive, a homogeneous state was utilized for simplification. By assuming that

Table 2 Cavitation CFD settings

Analysis type	Steady-state/transient
Vapour properties	$\rho_v = 2.1 \text{ kg}\cdot\text{m}^{-3}$, $\mu_v = 1.2\text{e}-5 \text{ Pa}\cdot\text{s}$
Saturation pressure(Pa)	110
Volume fraction of the nucleation site	$5\text{e}-4$
Initial bubble radius(m)	$1\text{e}-6$
Convergence target	RMS $1\text{e}-5$
Interface model	Frozen rotor/transient rotor-stator
Time step(s)	$1\text{e}-4$
Charging oil inlet	Opening boundary
F_{vap}	50
F_{cond}	0.01
f_{nuc}	$5\text{e}-4$
$R_B(\text{m})$	$1\text{e}-6$

the gas and the liquid phases have the same velocity and turbulence, the mixture of the two phases can be considered homogeneous, and the density and dynamic viscosity can be determined by the vapour volume fraction.

Although most of the cavitation CFD settings were the same as the non-cavitation model, the convergence target was relaxed to $1e-5$ for the cavitation model because the huge mixture density gradient deteriorated the convergence of the solution. The overall performance, such as component torques, were checked after the simulation to make sure they converged sufficiently. Furthermore, the steady-state cavitation model that provided the initial data for the transient calculation proved to improve the convergence effectively. Because the fluid domain of the torque converter is a closed loop (Figure 1), there is no inlet or outlet, and therefore the opening boundary was imposed on the charging oil inlet with a given static pressure. An appropriate time step was determined to capture the transient flow behaviour during one pump-turbine flow passage interaction in ten steps.

$$\Delta t = \frac{2\pi}{\omega_p - \omega_T} \cdot \frac{1}{Z_p} \cdot \frac{1}{10} = 1.2e-4 \text{ s}, \quad (5)$$

where ω_p and ω_T represent pump rotating speed and turbine rotating speed respectively, and Z_p is pump blade count.

The time step was taken as $1e-4$ s. A total of 300 time steps were calculated, during which the pump completed at least one revolution.

2.3 Experimental Setup

A torque converter dynamometer test cell was built to test the torque converter (Figure 4). The experimental setup consisted of a diesel engine, hydraulic supply system, test fixture, torque/speed sensors and absorbing dynamometer. A 588-kW diesel engine was used to drive the test rig, and a 1200-kW electric dynamometer was mounted to simulate the load. The hydraulic supply system allowed control of the oil temperature and the

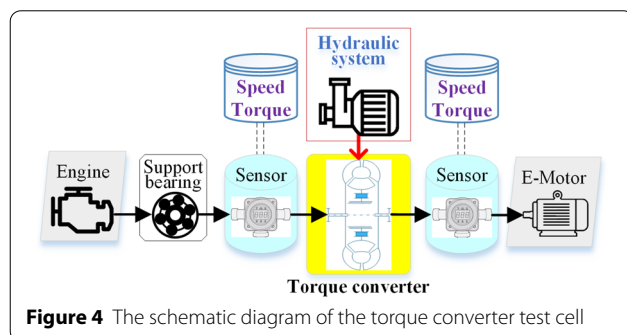


Figure 4 The schematic diagram of the torque converter test cell

charge pressure imposed upon the torque converter. The engine speed, i.e. the pump rotating speed, was stabilized at 2000 r/min throughout the test, and the turbine was held stationary by the motor to simulate the stall operating condition. The pump torque and the turbine torque were collected by torque sensors. The capacity constant (C) and the torque ratio (TR) could then be calculated as follows:

$$\begin{cases} C = \frac{T_p}{\omega_p^2 D^5}, \\ TR = \frac{T_T}{T_p}, \end{cases} \quad (6)$$

where T_p , T_T and T_s represent pump torque, turbine torque, and stator torque, respectively; D is torque converter torus diameter.

In order to distinguish the influence of charging oil pressures on torque converter cavitation, according to the actual working condition of the torque converter, the charge pressure was varied across three levels: 0.3, 0.6 and 0.9 MPa, during the test to evaluate the influence of charge pressure on the torque converter's overall hydrodynamic performance. The oil temperature was regulated at 90 °C, and the oil was supplied from different locations to evaluate the influence of oil feed location on hydrodynamic performance.

3 Results

3.1 CFD Model Validation

Figure 5 shows the results of the grid independence study that was performed on the steady-state CFD model to determine an appropriate grid density, and the torques derived from different mesh size models are listed in Table 3. It was found that 16 million elements would yield stable results. The mesh around the blades was further refined with a 12-layer prism grid to reduce the average y^+ value to less than two [30], enabling a low-Re

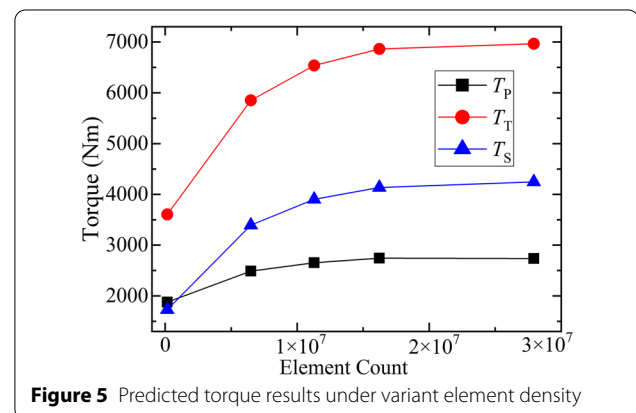


Figure 5 Predicted torque results under variant element density

Table 3 Grid independence study results

Mesh size (m)	Tot. elements	Pump torque		Turbine torque		Stator torque	
		T_p (N·m)	Div. (%)	T_T (N·m)	Div. (%)	T_s (N·m)	Div. (%)
0.06	164243	1877	32.6	3607	62.3	1729	96.3
0.0045	6489097	2489	6.6	5853	11.7	3394	15.0
0.0025	11279385	2653	3.4	6536	5.0	3903	5.9
0.0019	16228786	2743	— 0.3	6862	1.5	4135	2.7
0.0014	27921225	2735	—	6966	—	4246	—

Table 4 CFD predictions versus test data

	C ($\text{kg}\cdot\text{rad}^{-2}\cdot\text{m}^{-3}$)	C -error (%)	TR (N·m)	TR -error (%)
Test data	4.58	—	2.17	—
Non-cavitation	6.11	33.4	2.50	15.2
Steady-state cavitation	5.00	9.2	2.40	10.6
Transient cavitation	4.93	7.6	2.33	7.4
Cavitation effect	—	— 19.3	—	— 6.8

formulation of the SST model for precise near-wall flow predictions.

The 0.6 MPa charge pressure and S-P charging oil position were the conditions used to validate the CFD model. Table 4 compares the CFD results to the experimental data, showing that all of the CFD models overestimated the hydrodynamic performance. The non-cavitation CFD model, exhibited the largest deviation at stall operating condition, overestimating the capacity constant and the torque ratio by 33.4% and 15.2%, respectively. The corresponding deviations in the steady-state cavitation CFD model were 9.2% and 10.6%, and the transient cavitation model further reduced the prediction error to within 7.6% for both performance indices, indicating that the transient cavitation CFD model can predict the overall hydrodynamic performance with acceptable accuracy. Furthermore, the comparison between the non-cavitation CFD model and the cavitation CFD model confirmed that the torque converter suffered from heavy cavitation, and the differences in the deviations between the two models indicated the cavitation degree [[28]].

3.2 Effect of Charging Oil Configuration

The effect of the feed oil location was studied by applying the opening boundary condition with 0.6 MPa static pressure upon three different clearances. The results are listed in Table 5.

Table 5 Transient CFD predictions of hydrodynamic performance with different charging oil inlet configurations

Oil inlet	T_p (N·m)	T_T (N·m)	T_s (N·m)	C ($\text{kg}\cdot\text{rad}^{-2}\cdot\text{m}^{-3}$)	TR (N·m)
P-T clearance	1840.8	4460.8	2584.7	4.10	2.42
T-S clearance	2273.1	5387.1	3105.7	5.07	2.37
S-P clearance	2212.3	5149	2937	4.93	2.33

Table 6 Torque converter performance over variant charge pressure

Charge pressure	CFD model	T_p (N·m)	T_T (N·m)	C ($\text{kg}\cdot\text{rad}^{-2}\cdot\text{m}^{-3}$)	TR (N·m)
0.3 MPa	Non-cavitation	2741	6858	6.11	2.50
	cavitation	1983.7	4512.9	4.42	2.27
0.6 MPa	Non-cavitation	2743	6861.7	6.11	2.50
	cavitation	2212.3	5149	4.93	2.33
0.9 MPa	Non-cavitation	2746	6865.1	6.12	2.50
	cavitation	2477.8	5874	5.52	2.37

Table 5 shows that when the charging oil was supplied at the P-T clearance, the capacity constant was significantly lower and the torque ratio was slightly higher than when the oil was supplied at the other two clearances. Furthermore, when the oil was supplied from the stator inlet (T-S clearance), the capacity constant and the torque ratio were slightly higher than when the oil was supplied from the stator outlet (S-P clearance). These results suggest that the best method of supplying charging oil to the torque converter is at the T-S clearance, which showed less cavitation than the other two charging configurations.

3.3 Effect of Charge Pressure

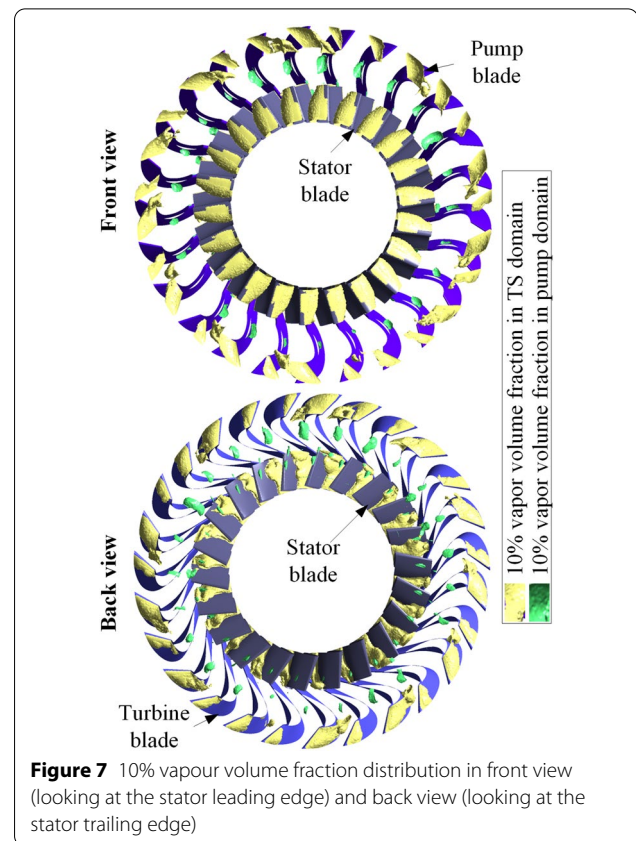
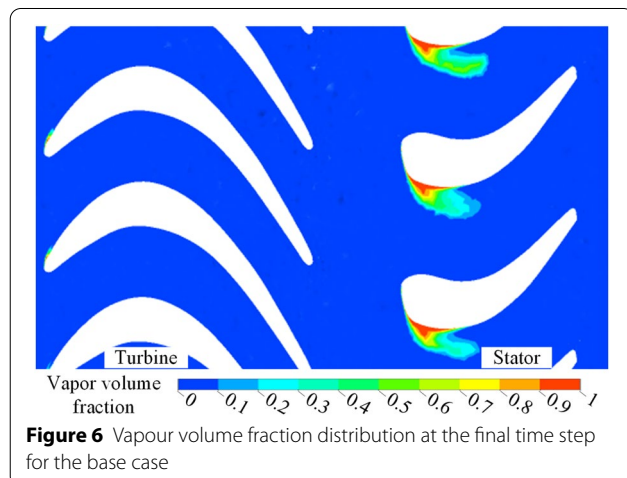
The effect of charge pressure was studied by varying the charge pressure imposed upon the S-P clearance at three different levels: 0.3, 0.6 and 0.9 MPa. The simulation results are reported in Table 6.

Table 6 shows that the charge pressure change did not affect the hydrodynamic performance for the non-cavitation simulations because the non-cavitation model only solved the incompressible fluid phase. However, the cavitation results indicated that increased charge pressure significantly improved the performance, implying that cavitation could be suppressed by increasing the charge pressure.

4 Discussion

The base case, with a charge pressure of 0.6 MPa and oil fed through the S-P clearance, was analysed to explore the transient cavitation behaviour in the torque converter. The CFD results indicated that cavitation in the base model brings about severe torque capacity loss. Table 4 shows that the torque converter suffered a reduction of 19.3% in the capacity constant, and the torque ratio also decreased by 6.8% because of cavitation. The cavitation bubbles blocked the main flow inside the torque converter, reducing the mass flow rate (Figures 6, 7, 8). The capacity of the torque converter is an indicator of power-absorbing ability, and a higher mass flow rate generally leads to higher capacity. Cavitation seriously degrades capacity when the bubbles block the main flow. The model showed that most of the vapour was generated at the stator nose on the suction side, and attached cavities can be found at the turbine nose (Figure 6).

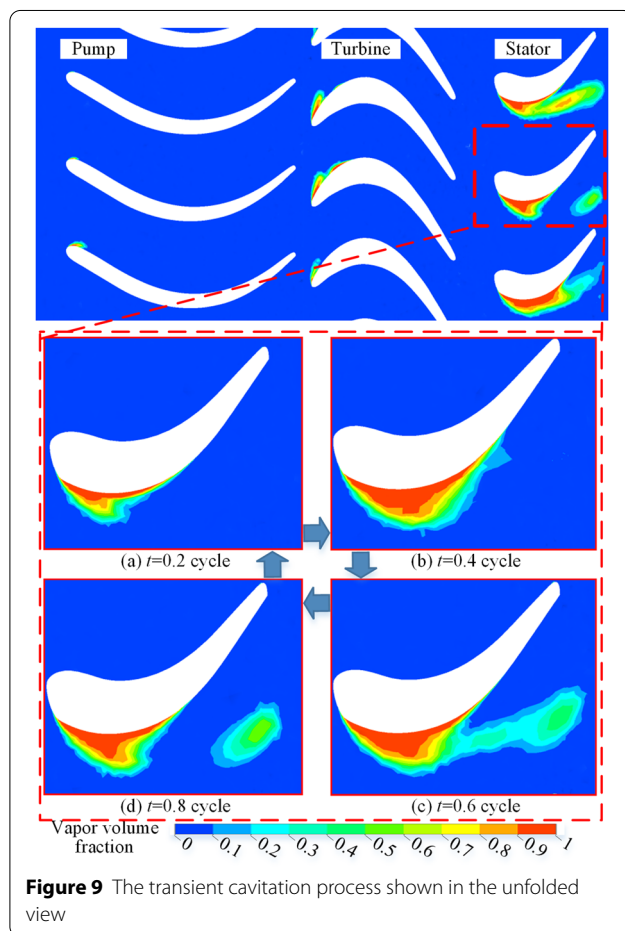
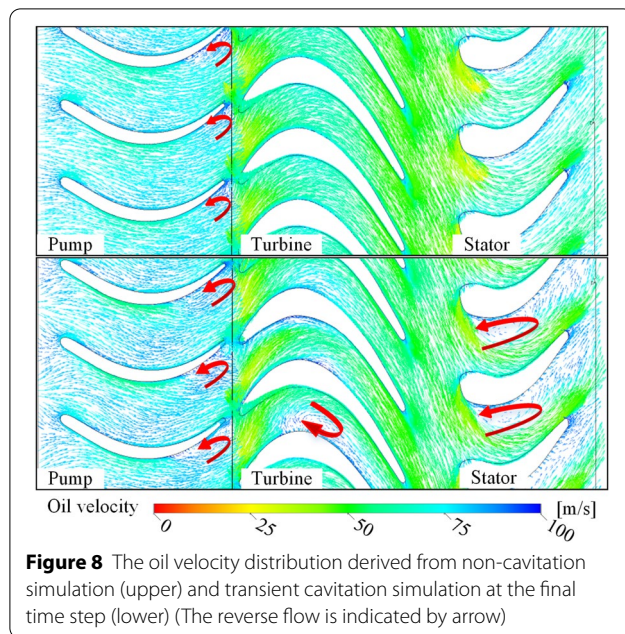
Although no measurable cavitation occurred in the pump domain, isolated cavitation bubbles that originated from cavity shedding in the stator domain were found in the pump domain (Figures 6, 7). As the fluid exiting the



pump struck the turbine cascade with a large incidence angle, small-scale attached cavities were generated at the turbine blade nose near the suction side (Figure 7). Cavitation was observed in the stator and the turbine domain. The cavities covered almost the entire stator nose, with scattered bubbles that detached from the stator domain entering the pump domain. However, these scattered bubbles collapsed soon after travelling to the latter part of the pump flow passage because of the high local pressure.

Figure 8 demonstrates that the oil velocity was relatively uniform for the non-cavitation case. Only a minor secondary flow region was found at the pump blade tail on the suction side. However, when cavitation was considered, much vapour was generated in the stator domain, leading to severe reverse flows in all three components. These reverse flows, along with the bubble blockage, significantly reduced the mass flow rate inside the torque converter, and consequently resulted in capacity loss.

The cavitation process inside the stator domain for the base case consisted of two types of cavitation: a stable sheet cavitation attached to the stator blade near the entrance and an unstable cavitation that tore part of the bubble and detached periodically. These cavitation types are shown in Figure 9, which depicts the transient



cavitation behaviour inside the stator domain. Cavitation vacancies formed on the stator suction side (Figure 9(a)) and grew towards the stator trailing edge (Figure 9(b)). When the vacancies reached the blade mid-span, a re-entrant jet, induced by the reverse flow and enhanced by the negative pressure gradient in the corresponding area, moved upstream from the blade end to the blade nose, splitting the cavity (Figure 9(c)). The shed cavity travelled downstream with the main flow, and the attached cavity shrank towards the blade nose (Figure 9(d)). This shedding process is repeated periodically.

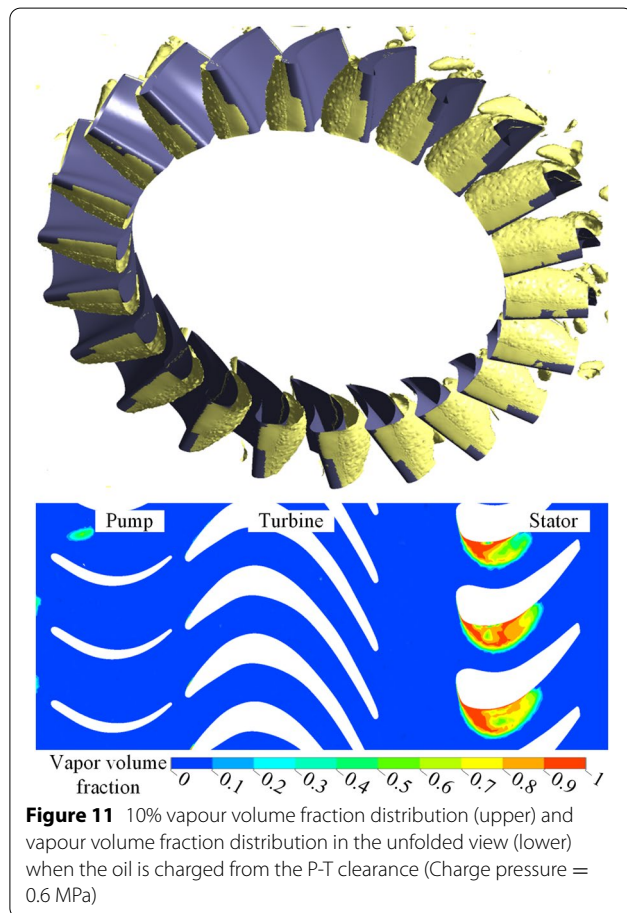
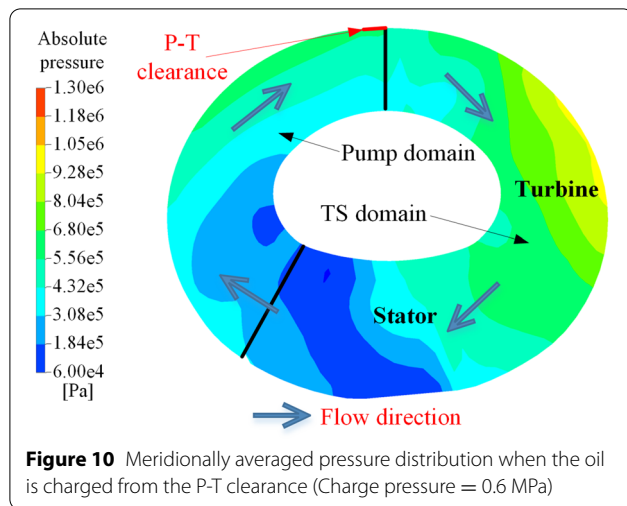
The investigation of the oil inlet position indicated that to suppress cavitation, the best location at which to supply the charging oil was the turbine-stator clearance, whereas pump-turbine clearance resulted in the highest torque capacity degradation. Two charging oil inlet arrangements were experimentally tested, and the results are compared with numerical predictions in Table 7. The predictions agreed fairly well with the test data, and the numerical and the experimental results both indicated that supplying the oil from the T-S clearance resulted in higher capacity, i.e., less cavitation.

As the generation and collapse of cavities were simulated by a homogeneous cavitation model, no interface between the two phases was calculated, and the vapour was characterized by the vapour volume fraction within the homogeneous mixture. The cavitation processes under the three different charging oil configurations were visualized using a 10% vapour volume fraction iso-surface distribution in the stator domain and the vapour volume fraction distribution in the unfolded view. The averaged absolute pressure distributions in the meridional view were also shown to illustrate the influence of the oil feed position. The cavitation region was mainly located in the front part of the stator passage in all the three cases.

Figure 10 illustrates the meridionally averaged pressure distribution when the oil was fed through the P-T clearance with 0.6 MPa pressure. The absolute pressure in the turbine domain was clearly the highest among all components, and the stator pressure was the lowest. A significant pressure gradient can be observed in the whole

Table 7 The numerical and experimental torque converter stall performance over different charging oil inlet arrangements (Charge pressure = 0.6 MPa)

Oil inlet		C (kg·rad ⁻² ·m ⁻³)	C -error (%)	TR (N·m)	TR -error (%)
T-S clearance	Test	4.75	–	2.19	–
	CFD	5.07	6.7	2.37	8.2
S-P clearance	Test	4.58	–	2.17	–
	CFD	4.93	7.6	2.33	7.4



fluid domain, and the large-scale low-pressure region in the stator domain gave rise to cavitation.

Figure 11 shows that when the charging oil was supplied to the torque converter through the P-T clearance, significant cavitation took place in the stator domain.

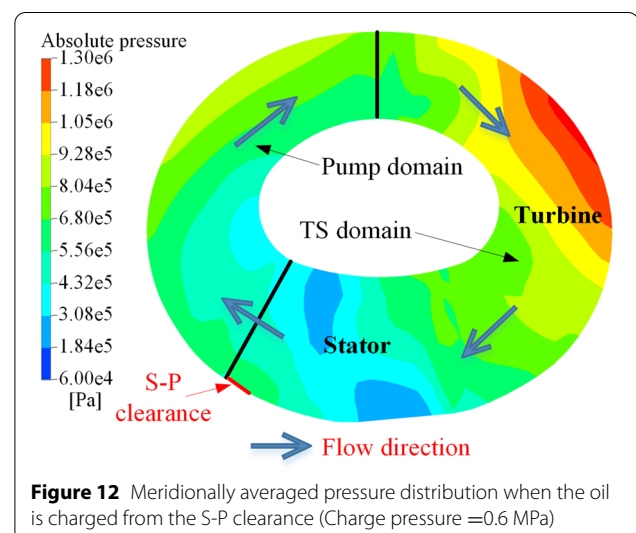
The cavitation vacancies covered the entire stator nose and spread into the stator midspan. These large cavities blocked the main flow and drastically degraded capacity. No cavitation could be found in the turbine domain as a result of the high pressure of the oil supplied at the turbine inlet, which led to a relatively higher torque ratio compared to the other two cases (Table 5).

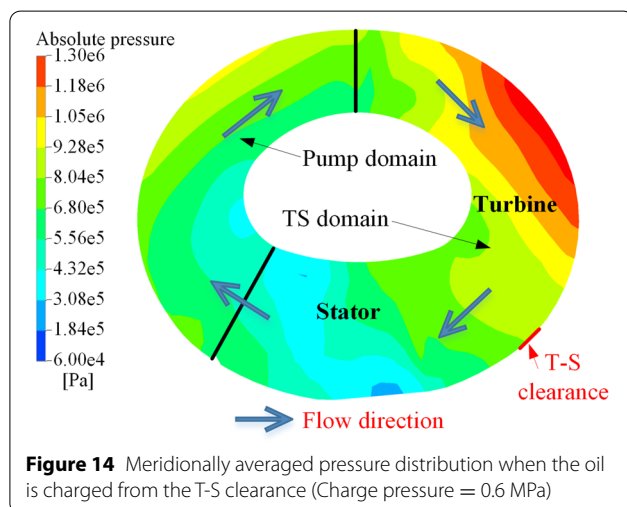
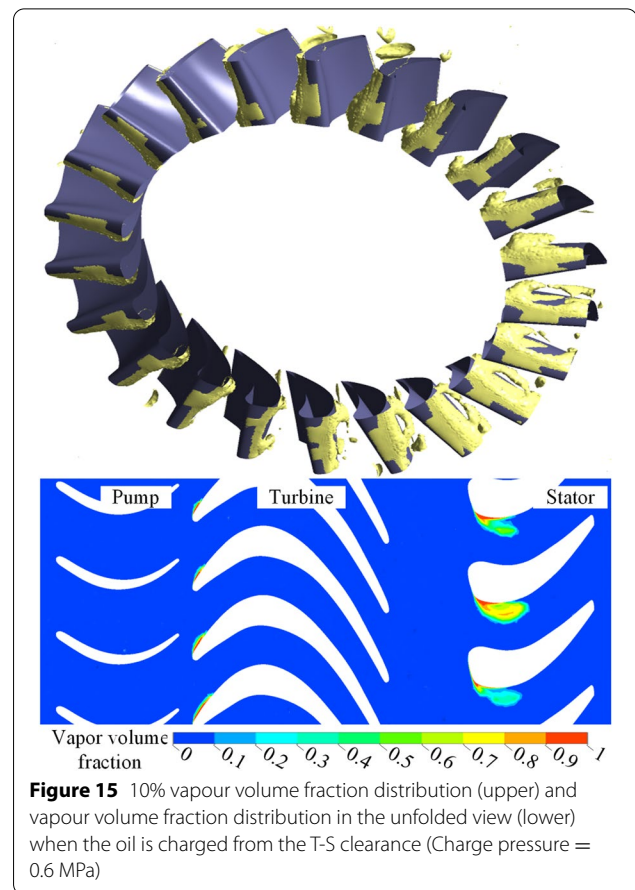
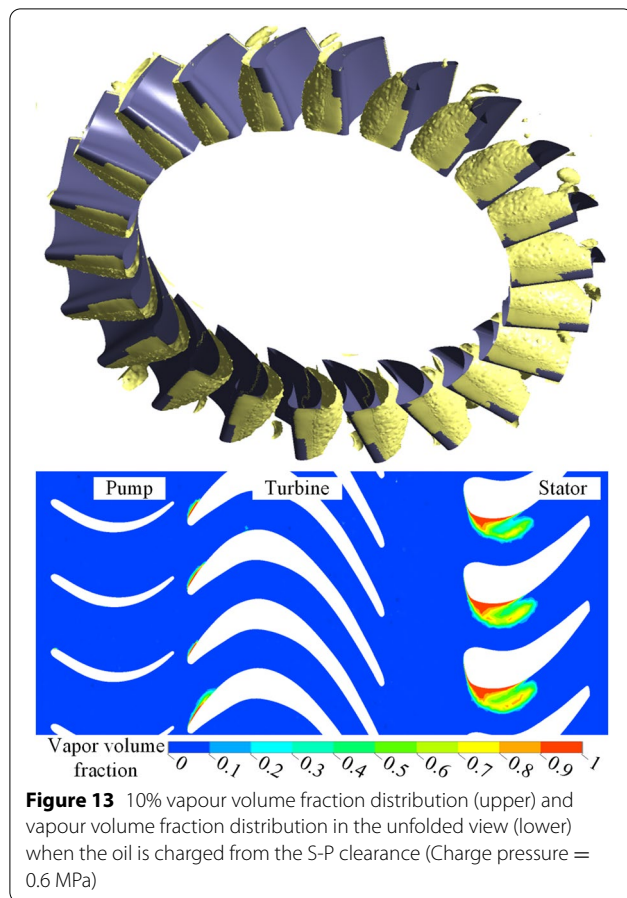
The meridionally averaged pressure for the S-P feed oil location case is depicted in Figure 12, which shows a high-pressure region in the turbine domain near the shroud. Although the pressure distribution pattern was similar to the P-T feed oil location case, the overall pressure level was greatly increased compared to the P-T clearance case (Figure 10).

Figure 13 shows that when the oil was supplied from through the S-P clearance, the cavitation region shrank towards the stator blade leading edge, and consequently reduced the amount of cavitation. However, the cavities still covered almost the entire stator blade nose, and small cavities were observed in the turbine domain as the high-velocity fluid struck the turbine blade, which contributed to the torque ratio degradation.

The averaged pressure distribution in the T-S case (Figure 14) is almost the same as that in the S-P case (Figure 12). However, as the high-pressure oil was supplied to the inlet of the stator, the overall pressure level in the stator domain was slightly higher and the low-pressure region was smaller.

Figure 15 reveals that, when the oil was supplied from the T-S clearance, the cavitation region further shrank towards the stator blade leading edge and barely covered the stator nose. Because the cavitation started at the stator nose, when high-pressure oil was supplied to the stator inlet, cavitation and the associated capacity





loss were partially suppressed. However, small cavities remained in the turbine flow passages, indicating that the cavitation condition in the turbine domain was not improved in this case.

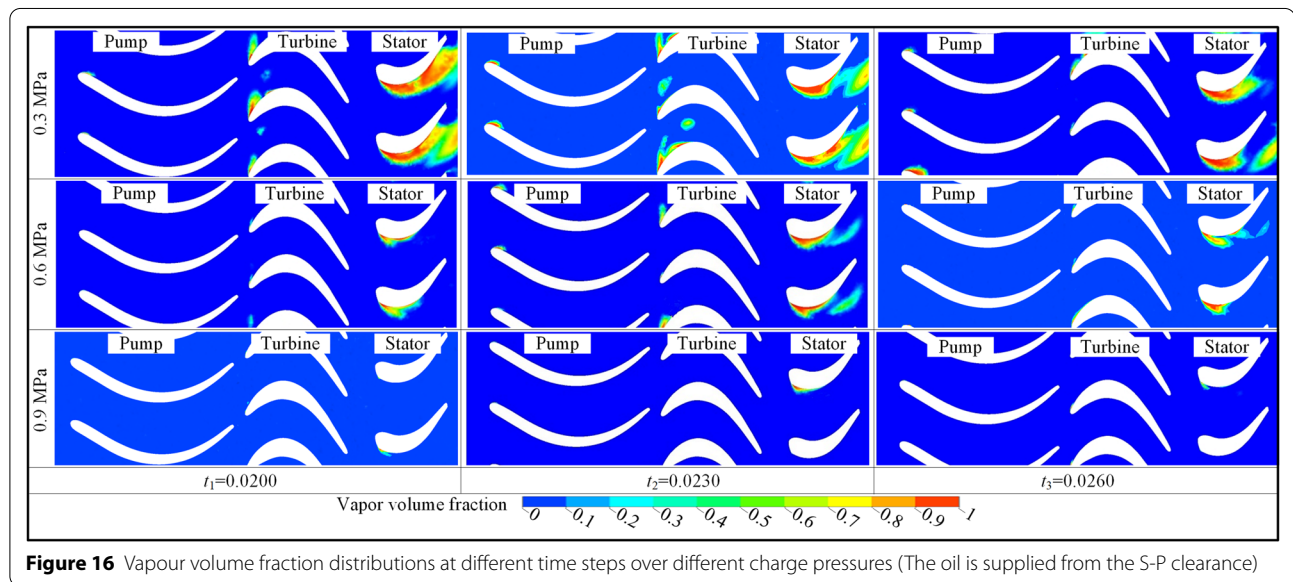
The investigation of the charge pressure effect shows that the performance degradation decreased with an increasing charge pressure. The reason for this is straightforward: higher charge pressure increases the overall pressure level inside the torque converter and suppresses the cavitation process. The numerical predictions are compared to the test data in Table 8.

It is clear from both the numerical and the experimental results that the capacity constant increased as the charge pressure increased. The numerical results show that the torque ratio increased slightly with an increasing charge pressure, however, the test results prove that the charge pressure does not have a significant effect on the torque ratio.

The vapour volume fraction distributions shown in Figure 16 indicate that charge pressure has a significant effect on the cavitation degree and the cavitation form. The figure shows significant reduction in the cavitation region as the charge pressure increases. For all three charge pressure settings, cavitation mainly occurred in the stator domain, and all cavitation originated on the suction side of stator blade near the nose, where the flow exiting the turbine struck

Table 8 The numerical and experimental torque converter stall performance over various charge pressures (Oil is charged from the S-P clearance)

Charge pressure		C (kg·rad ² ·m ⁻³)	C -error (%)	TR (N·m)	TR -error (%)
0.3 MPa	Test	4.43	–	2.19	–
	CFD	4.42	– 0.2	2.27	3.7
0.6 MPa	Test	4.58	–	2.17	–
	CFD	4.93	7.6	2.33	7.4
0.9 MPa	Test	4.97	–	2.18	–
	CFD	5.52	11.1	2.37	8.7

**Figure 16** Vapour volume fraction distributions at different time steps over different charge pressures (The oil is supplied from the S-P clearance)

the stator cascade with a big incidence angle and velocity. Severe unsteady cavitation could also be found in the turbine under the 0.3 MPa charge pressure. However, only scattered small scale cavities were generated in the turbine under higher charge pressure conditions. The degree of cavitation decreased with an increasing charge pressure, leading to lower capacity degradation. It was found that the cavitation flows under 0.3 MPa and 0.6 MPa were quite unsteady, particularly those flows in the stator domain. When the charge pressure was further increased to 0.9 MPa, the cavitation in the pump and the turbine domain was almost eliminated; moreover, in the stator domain, the cavitation switched from unsteady shedding cavitation to steady attached cavitation and the cavitation region shrank drastically towards the stator nose.

The cavitation potential can be characterized by a non-dimensional cavitation number σ . When σ drops below a critical level, cavitation occurs, such that lower σ implies a higher degree of cavitation. This value is calculated as follows:

$$\sigma = \frac{p_{\text{ref}} - p_v}{0.5 \rho_1 v_{\text{ref}}^2}, \quad (7)$$

where p_{ref} represents the charge pressure, and v_{ref} is the equivalent average velocity inside the torque converter, which directly correlated to the mass flow rate, given as

$$v_{\text{ref}} = \frac{MF}{A \rho_1}, \quad (8)$$

where MF is mass flow rate, A is constant throughout the whole flow passage and $A = 2.7 \times 10^{-2} \text{ m}^2$ in this model.

The cavitation numbers for all the cases are shown in Table 9 and Figure 17. These results indicated that for a given charge oil inlet configuration, the cavitation number corresponded to the cavitation potential. The cavitation number decreased along with the charge pressure, resulting in more cavitation. However, cavitation number is not useful for assessing cavitation degree among different charge oil configurations. For instance, although

Table 9 Cavitation numbers under various charging conditions

Charging position	Charge pressure (MPa)	Mass flow rate(kg·s ⁻¹)	Cavitation number
S-P clearance	0.3	330.8	3.343
S-P clearance	0.6	386.1	4.909
S-P clearance	0.9	407.4	6.614
P-T clearance	0.6	311.2	7.556
T-S clearance	0.6	390.1	4.811

the cavitation number for the P-T clearance case ranked the highest among all calculated samples (Figure 17), this case suffered from severe cavitation. The P-T clearance was located at the largest radius of the torus (Figure 1), and the pressure dropped significantly with a decreasing torus radius as a result of decreased centrifugal pressure (Figure 10). However, cavitation mainly occurred inside the stator domain, which had the lowest torus radius among all three components. Contrary to those results, the cavitation number for the T-S clearance case was slightly lower than that of the S-P clearance, even though the cavitation degree in the T-S clearance case was lower than that in the S-P clearance because high-pressure oil was supplied near the cavitation region.

5 Conclusions

This study investigated the transient cavitation behaviour in a torque converter at stall operating condition through a full three-dimensional CFD model. The turbine and the stator were united as one domain to simplify the simulation. The model was validated against experimental data, and the effects of the charging oil pressure and feed location were investigated.

Cavitation inside the torque converter brought about severe performance degradation, especially in terms of the torque capacity. For the base case, the

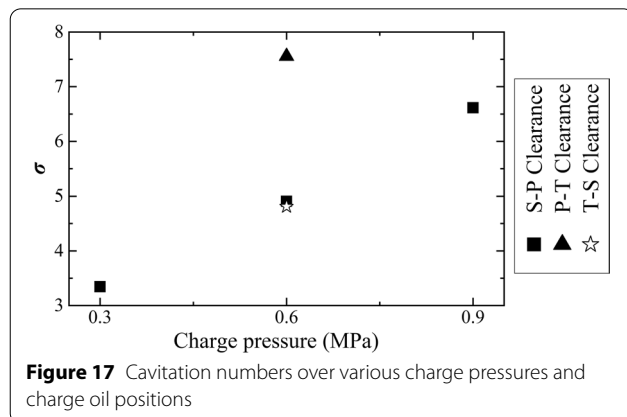
non-cavitation CFD simulation overpredicted the capacity constant by 33.4% compared to the experimental results, whereas the cavitation CFD model limited the deviation to within 7.6%. The comparison between the non-cavitation and the cavitation calculations could be used to determine the cavitation degree, and thereby provide engineers with useful tools for the consideration of cavitation. The charging oil feed location had a significant effect on the cavitation characteristics inside the torque converter. Supplying the oil from the P-T clearance led to lower pressure inside the stator domain and consequently resulted in heavy cavitation. The charging oil feed location in terms of cavitation suppression was the T-S clearance, i.e., the stator inlet. Because cavitation mainly originated at the stator nose, supplying high-pressure oil to the stator inlet raised the average local pressure at the corresponding area and thus suppressed cavitation.

The charge pressure also significantly influenced the cavitation degree at the stall operating condition. The numerical and experimental studies both revealed that higher charge pressures increased the overall pressure level inside the torque converter and consequently suppressed cavitation. The transient CFD model revealed that cavities were periodically shed in both the turbine and stator domains when the charge pressure was insufficient. Increasing the charge pressure first eliminated the cavitation bubbles in the turbine and pump domains, and further increases in charge pressure led to cavitation suppression in the stator domain.

The proposed CFD model agreed fairly well with the experimental results; however, this study addressed only the influence of cavitation on external hydrodynamic performance. Cavitation bubble visualization and more sophisticated measurements, such as internal pressure, noise, and vibration tests, would be required to validate the cavitating flow behaviour. Furthermore, the numerical error increased with an increasing charge pressure, mainly because of the inconsistency between the CFD boundary settings and the test conditions. In order to improve the simulation accuracy, internal fluid flow measurements are necessary. The pressure level can be measured via micro-scale pressure sensors, and the measured pressure can be imposed upon the CFD boundary to increase the model fidelity. This will be a subject of future work.

Abbreviations

f_l : Liquid volume fraction; ρ_l : Liquid density (kg·m⁻³); v_l : Velocity (m·s⁻¹); \dot{m} : Interphase mass transfer per unit (kg·s⁻¹); R_B : Bubble radius (m); p_v : Vapour pressure (Pa); p : Local pressure (Pa); f_v : Vapour volume fraction; ρ_v : Vapour density (kg·m⁻³); f_{nu} : Volume fraction of the nucleation site; F_{vap} : Vapourization constant; F_{cond} : Condensation constant; T_p : Pump torque (N·m); T_t : Turbine torque (N·m); T_s : Stator torque (N·m); C : Capacity constant (kg·rad⁻²·m⁻³); ω_p :



Pump rotating speed ($\text{rad}\cdot\text{s}^{-1}$); ω_T : Turbine rotating speed ($\text{rad}\cdot\text{s}^{-1}$); Z_p : Pump blade count; D : Torque converter torus diameter (m); TR : Torque ratio; σ : Cavitation number; p_{ref} : Reference pressure (Pa); v_{ref} : Reference velocity ($\text{m}\cdot\text{s}^{-1}$); MF : Mass flow rate ($\text{kg}\cdot\text{s}^{-1}$); A : Toroidal area (m^2).

Acknowledgements

The authors sincerely thanks to Professor Houston G. Wood of the University of Virginia for his critical discussion and reading during manuscript preparation.

Authors' Information

Cheng Liu, born in 1986, is currently an assistant professor at *Beijing Institute of Technology, China*. He received his PhD degree from *Beijing Institute of Technology, China*, in 2015. His research interests include vehicle hybrid technology, fluid transmission and control, transient cavitation and control.

Meng Guo, born in 1991, is currently a PhD candidate at *School of Mechanical Engineering, Beijing Institute of Technology, China*. He received his master's degree from *Yanshan University, China*, in 2018. His research interests include fluid transmission and control, transient cavitation and fluid-structure interaction.

Qingdong Yan, born in 1964, is currently a professor at *Beijing Institute of Technology, China*. He received his PhD degree from *Beijing Institute of Technology, China*, in 1995. His research interests include vehicle system integration technology, vehicle transmission and control technology, fluid machinery and CFD.

Wei Wei, born in 1978, is currently an associate professor at *Beijing Institute of Technology, China*. He received his PhD degree from *Beijing Institute of Technology, China*, in 2006. His research interests include modern design method of vehicle transmission system, theory and technology of vehicle automatic transmission system, design theory and test of hydraulic components.

Authors contributions

CL performed the data analyses, designed and performed the experiments, and wrote the manuscript; MG contributed significantly to analysis and manuscript preparation; QY contributed to the conception of the study; WW helped perform the analysis with constructive discussions. All authors read and approved the final manuscript.

Funding

Supported by National Natural Science Foundation of China (Grant Nos. 51805027, 51475041), Beijing Institute of Technology Research Fund Program for Young Scholars (Grant No. 303001181804) and Vehicular Transmission Key Laboratory Fund.

Competing interests

The authors declare no competing financial interests.

Author Details

¹School of Mechanical Engineering, Beijing Institute of Technology, Beijing 100081, China. ²Chongqing Innovation Center, Beijing Institute of Technology, Chongqing 401122, China. ³Advanced Technology Research Institute, Beijing Institute of Technology, Jinan 250307, China.

Received: 7 May 2020 Revised: 28 March 2022 Accepted: 11 April 2022
Published online: 04 May 2022

References

- Y Yang, W W Liou, F Qureshi, et al. Transmission fluid properties' effects on performance characteristics of a torque converter: A computational study. *Tribology Transactions*, 2021, 64(6): 1055-1063.
- Q D Yan, W Wei, C Liu. Development and prospect of hydrodynamic power transmission technology. *Hydraulics Pneumatics & Seals*, 2021, 41(2): 1-8. (in Chinese)
- T Usui, T Okaji, T Muramatsu, et al. Development of a compact ultra-flat torque converter equipped with a high-performance damper. *SAE Technical Paper*, 2015-01-1088, 2015.
- C Liu, Q D Yan, J Li, et al. Investigation on the cavitation characteristics of high power-density torque converter. *Journal of Mechanical Engineering*, 2020, 56(24): 147-155. (in Chinese)
- C B Liu, C Sheng, H Yang, et al. Design and optimization of bionic Janus blade in hydraulic torque converter for drag reduction. *Journal of Bionic Engineering*, 2018, 15: 160-172.
- Q P Chen, M M Wu, S Kang, et al. Study on cavitation phenomenon of twin-tube hydraulic shock absorber based on CFD. *Engineering Applications of Computational Fluid Mechanics*, 2019, 13(1): 1049-1062.
- H Kobayashi, R Hagiwara, S Kawasaki, et al. Numerical analysis of suppression effect of asymmetric slit on cavitation instabilities in cascade. *Journal of Fluids Engineering*, 2018, 140(2): 021302.
- J Wang, Y Wang, H L Liu, et al. Rotating corrected-based cavitation model for a centrifugal pump. *Journal of Fluids Engineering*, 2018, 140(11): 111301.
- L L Geng, X Escaler. Assessment of RANS turbulence models and Zwart cavitation model empirical coefficients for the simulation of unsteady cloud cavitation. *Engineering Applications of Computational Fluid Mechanics*, 2020, 14(1): 151-167.
- H Shim, K Kim, Y Choi. Three-objective optimization of a centrifugal pump to reduce flow recirculation and cavitation. *Journal of Fluids Engineering*, 2018, 140(9): 091202.
- X M Liu, Z H Wu, B B Li, et al. Influence of inlet pressure on cavitation characteristics in regulating valve. *Engineering Applications of Computational Fluid Mechanics*, 2020, 14(1): 299-310.
- C B Liu, Z Xu, W Ma, et al. CFD investigating medium-temperature influences on performance prediction and structure stress calculation in a hydrodynamic torque converter. *Numerical Heat Transfer: Part A, Applications*, 2017 72(7): 563-578.
- Y Dong, V Korivi, P Attibele, et al. Torque converter CFD engineering part II: Performance improvement through core leakage flow and cavitation control. *SAE Technical Paper*, 2002-01-0884, 2002.
- D L Robinette. *Detecting and predicting the onset of cavitation in automotive torque converters*. Ph.D. Dissertation, Michigan Technological University, Houghton, MI. 2007.
- P Xiong, X Y Chen, H J Sun, et al. Effect of the blade shaped by Joukowski airfoil transformation on the characteristics of the torque converter. *Proc IMechE Part D: J Automobile Engineering*, 2021, 235(14): 3314-3321.
- C Walber, J R Blough, M Johnson, et al. Measuring and comparing frequency response functions of torque converter turbines submerged in transmission fluid. *SAE Technical Paper*, 2011-01-1662, 2011.
- D L Robinette, J M Schweitzer, D G Maddock, et al. Predicting the onset of cavitation in automotive torque converters – Part II: A generalized model. *International Journal of Rotating Machinery*, 2008: 803940.
- C D Reynolds. *Characterization of torque converter cavitation sound power level over varying speed ratio*. Houghton: Michigan Technological University, 2016.
- S Watanabe, R Otani, S Kunimoto, et al. Vibration characteristics due to cavitation in stator element of automotive torque converter at stall condition. *ASME Paper*, 2013, No. FEDSM2012-72418, 535-541. <https://doi.org/10.1115/FEDSM2012-72418>
- Q D Yan, Z M Song, W Wei, et al. Pressure measurement and analysis of stator blade surface of hydrodynamic torque converter. *Journal of Mechanical Engineering*, 2019, 55(10): 115-121. (in Chinese)
- E D J Rivera. *Pressure measurements inside multiple cavities of a torque converter and CFD correlation*. Houghton: Michigan Technological University, 2018.
- J Ju, J Jang, M Choi, et al. Effects of cavitation on performance of automotive torque converter. *Advances in Mechanical Engineering*, 2016, 8(6): 1-9. DOI: <https://doi.org/10.1177/1687814016654045>
- K Tsutsumi, S Watanabe, S Tsuda, et al. Cavitation simulation of automotive torque converter using a homogeneous cavitation model. *European Journal of Mechanics B/Fluids*, 2017, 61(2): 263-270. DOI: <https://doi.org/10.1016/j.euromechflu.2016.09.001>
- T Usui, Y Iga. Prediction method of cavitation inside torque converter using gaseous cavitation model. *Jidōsha Gijyutsukai ronbunshū*, 2021, 52(5): 961-966. (in Japanese)

- [25] C Liu, W Wei, Q D Yan, et al. Torque converter capacity improvement through cavitation control by design. *Journal of Fluids Engineering*, 2017, 139(4): 041103.
- [26] C Liu, W Wei, Q D Yan, et al. Influence of stator blade geometry on torque converter cavitation. *Journal of Fluids Engineering*, 2018, 140(4): 041102.
- [27] C Liu, W Wei, Q D Yan, et al. On the application of passive flow control for cavitation suppression in torque converter stator. *International Journal of Numerical Methods for Heat & Fluid Flow*, 2019, 29(1): 204-222.
- [28] M Guo, C Liu, Q D Yan, et al. The effect of rotating speeds on the cavitation characteristics in hydraulic torque converter. *Machines*, 2022, 10(2): 80.
- [29] Bakir, R Rey, A G Gerber, et al. Numerical and experimental investigations of the cavitating behaviour of an inducer. *International Journal of Rotating Machinery*, 2004, 10(1): 15-25.
- [30] M Guo, C Liu, Q D Yan, et al. Evaluation and validation of viscous oil cavitation model used in torque converter. *Applied sciences*, 2021, 11(8): 3643.

Submit your manuscript to a SpringerOpen[®] journal and benefit from:

- Convenient online submission
- Rigorous peer review
- Open access: articles freely available online
- High visibility within the field
- Retaining the copyright to your article

Submit your next manuscript at ► [springeropen.com](https://www.springeropen.com)